

Evidence of Intermediate-Scale Energy Spectrum Anisotropy of Cosmic Rays $E \geq 10^{19.2}$ eV with the Telescope Array Surface Detector

R.U. ABBASI,¹ M. ABE,² T. ABU-ZAYYAD,¹ M. ALLEN,¹ R. AZUMA,³ E. BARCIKOWSKI,¹ J.W. BELZ,¹ D.R. BERGMAN,¹ S.A. BLAKE,¹ R. CADY,¹ B.G. CHEON,⁴ J. CHIBA,⁵ M. CHIKAWA,⁶ A. DI MATTEO,⁷ T. FUJII,⁸ K. FUJITA,⁹ M. FUKUSHIMA,^{8,10} G. FURLICH,¹ T. GOTO,⁹ W. HANLON,¹ M. HAYASHI,¹¹ Y. HAYASHI,⁹ N. HAYASHIDA,¹² K. HIBINO,¹² K. HONDA,¹³ D. IKEDA,⁸ N. INOUE,² T. ISHII,¹³ R. ISHIMORI,³ H. ITO,¹⁴ D. IVANOV,¹ H.M. JEONG,¹⁵ S.M. JEONG,¹⁵ C.C.H. JUI,¹ K. KADOTA,¹⁶ F. KAKIMOTO,³ O. KALASHEV,¹⁷ K. KASAHARA,¹⁸ H. KAWAI,¹⁹ S. KAWAKAMI,⁹ S. KAWANA,² K. KAWATA,⁸ E. KIDO,⁸ H.B. KIM,⁴ J.H. KIM,¹ J.H. KIM,²⁰ S. KISHIGAMI,⁹ S. KITAMURA,³ Y. KITAMURA,³ V. KUZMIN,^{17,*} M. KUZNETSOV,¹⁷ Y.J. KWON,²¹ K.H. LEE,¹⁵ B. LUBSANDORZHIEV,¹⁷ J.P. LUNDQUIST,¹ K. MACHIDA,¹³ K. MARTENS,¹⁰ T. MATSUYAMA,⁹ J.N. MATTHEWS,¹ R. MAYTA,⁹ M. MINAMINO,⁹ K. MUKAI,¹³ I. MYERS,¹ K. NAGASAWA,² S. NAGATAKI,¹⁴ R. NAKAMURA,²² T. NAKAMURA,²³ T. NONAKA,⁸ A. NOZATO,⁶ H. ODA,⁹ S. OGIO,⁹ J. OGURA,³ M. OHNISHI,⁸ H. OHOKA,⁸ T. OKUDA,²⁴ Y. OMURA,⁹ M. ONO,¹⁴ R. ONOGI,⁹ A. OSHIMA,⁹ S. OZAWA,¹⁸ I.H. PARK,¹⁵ M.S. PSIRKOV,^{17,25} D.C. RODRIGUEZ,¹ G. RUBTSOV,¹⁷ D. RYU,²⁰ H. SAGAWA,⁸ R. SAHARA,⁹ K. SAITO,⁸ Y. SAITO,²² N. SAKAKI,⁸ N. SAKURAI,⁹ L.M. SCOTT,²⁶ T. SEKI,²² K. SEKINO,⁸ P.D. SHAH,¹ F. SHIBATA,¹³ T. SHIBATA,⁸ H. SHIMODAIRA,⁸ B.K. SHIN,⁹ H.S. SHIN,⁸ J.D. SMITH,¹ P. SOKOLSKY,¹ B.T. STOKES,¹ S.R. STRATTON,^{1,26} T.A. STROMAN,¹ T. SUZAWA,² Y. TAKAGI,⁹ Y. TAKAHASHI,⁹ M. TAKAMURA,⁵ M. TAKEDA,⁸ R. TAKEISHI,¹⁵ A. TAKETA,²⁷ M. TAKITA,⁸ Y. TAMEDA,²⁸ H. TANAKA,²⁹ M. TANAKA,³⁰ S.B. THOMAS,¹ G.B. THOMSON,¹ P. TINYAKOV,^{17,7} I. TKACHEV,¹⁷ H. TOKUNO,³ T. TOMIDA,²² S. TROITSKY,¹⁷ Y. TSUNESADA,³ K. TSUTSUMI,³ Y. UCHIHORI,³¹ S. UDO,¹² F. URBAN,³² T. WONG,¹ M. YAMAMOTO,²² R. YAMANE,⁹ H. YAMAOKA,³⁰ K. YAMAZAKI,¹² J. YANG,³³ K. YASHIRO,⁵ Y. YONEDA,⁹ S. YOSHIDA,¹⁹ H. YOSHII,³⁴ Y. ZHEZHER,¹⁷ AND Z. ZUNDEL¹

¹High Energy Astrophysics Institute and Department of Physics and Astronomy, University of Utah, Salt Lake City, Utah, USA

²The Graduate School of Science and Engineering, Saitama University, Saitama, Saitama, Japan

³Graduate School of Science and Engineering, Tokyo Institute of Technology, Meguro, Tokyo, Japan

⁴Department of Physics and The Research Institute of Natural Science, Hanyang University, Seongdong-gu, Seoul, Korea

⁵Department of Physics, Tokyo University of Science, Noda, Chiba, Japan

⁶Department of Physics, Kinki University, Higashi Osaka, Osaka, Japan

⁷Service de Physique Thorique, Universit Libre de Bruxelles, Brussels, Belgium

⁸Institute for Cosmic Ray Research, University of Tokyo, Kashiwa, Chiba, Japan

⁹Graduate School of Science, Osaka City University, Osaka, Osaka, Japan

¹⁰Kavli Institute for the Physics and Mathematics of the Universe (WPI), Todai Institutes for Advanced Study, University of Tokyo, Kashiwa, Chiba, Japan

¹¹Information Engineering Graduate School of Science and Technology, Shinshu University, Nagano, Nagano, Japan

¹²Faculty of Engineering, Kanagawa University, Yokohama, Kanagawa, Japan

¹³Interdisciplinary Graduate School of Medicine and Engineering, University of Yamanashi, Kofu, Yamanashi, Japan

¹⁴Astrophysical Big Bang Laboratory, RIKEN, Wako, Saitama, Japan

¹⁵Department of Physics, Sungkyunkwan University, Jang-an-gu, Suwon, Korea

¹⁶Department of Physics, Tokyo City University, Setagaya-ku, Tokyo, Japan

¹⁷Institute for Nuclear Research of the Russian Academy of Sciences, Moscow, Russia

¹⁸Advanced Research Institute for Science and Engineering, Waseda University, Shinjuku-ku, Tokyo, Japan

¹⁹Department of Physics, Chiba University, Chiba, Chiba, Japan

²⁰Department of Physics, School of Natural Sciences, Ulsan National Institute of Science and Technology, UNIST-gil, Ulsan, Korea

²¹Department of Physics, Yonsei University, Seodaemun-gu, Seoul, Korea

²²Academic Assembly School of Science and Technology Institute of Engineering, Shinshu University, Nagano, Nagano, Japan

²³Faculty of Science, Kochi University, Kochi, Kochi, Japan

²⁴Department of Physical Sciences, Ritsumeikan University, Kusatsu, Shiga, Japan

²⁵Sternberg Astronomical Institute, Moscow M.V. Lomonosov State University, Moscow, Russia

²⁶Department of Physics and Astronomy, Rutgers University - The State University of New Jersey, Piscataway, New Jersey, USA

²⁷Earthquake Research Institute, University of Tokyo, Bunkyo-ku, Tokyo, Japan

²⁸Department of Engineering Science, Faculty of Engineering Osaka Electro-Communication University, Osaka, Osaka, Japan

²⁹Graduate School of Information Sciences, Hiroshima City University, Hiroshima, Hiroshima, Japan

³⁰Institute of Particle and Nuclear Studies, KEK, Tsukuba, Ibaraki, Japan

³¹*National Institute of Radiological Science, Chiba, Chiba, Japan*

³²*Central European Institute for Cosmology and Fundamental Physics, Institute of Physics, Czech Academy of Sciences, Na Slovance 1999/2 Prague, Czech Republic*

³³*Department of Physics and Institute for the Early Universe, Ewha Womans University, Seodaaemun-gu, Seoul, Korea*

³⁴*Department of Physics, Ehime University, Matsuyama, Ehime, Japan*

Submitted to ApJL

ABSTRACT

An intermediate-scale energy spectrum anisotropy has been found in the arrival directions of ultra-high energy cosmic rays of energies above $10^{19.2}$ eV in the northern hemisphere, using 7 years of data from the Telescope Array (TA) surface detector (SD). A relative energy distribution test is done comparing events inside oversampled spherical cap bins of equal exposure, to those outside, using the Poisson likelihood ratio test. The center of maximum significance is at 9^h16^m , 45° . and has a deficit of events with energies $10^{19.2} \leq E < 10^{19.75}$ eV and an excess for $E \geq 10^{19.75}$ eV. The post-trial probability of this energy anisotropy, appearing by chance anywhere on an isotropic sky, is found by Monte Carlo (MC) simulation to be 9×10^{-5} ($3.74\sigma_{\text{global}}$).

Keywords: astroparticle physics, cosmic rays, large-scale structure of universe

1. INTRODUCTION

The sources of Ultra-high energy cosmic rays (UHECR) are still unknown though at energies above 10^{19} eV the lack of strong anisotropy makes it very improbable that they are of galactic origin. Because of the interactions of cosmic ray particles with the infrared and microwave background radiation, the distribution of UHECR sources should be limited to distances smaller than 100 Mpc for protons and iron and 20 Mpc for intermediate mass nuclei like helium/oxygen/carbon/nitrogen (Kotera & Olinto (2011)). The number of possible accelerators in this volume is limited by energy considerations to galaxy clusters, supermassive black holes in active galaxies (AGNs), jets and lobes of active galaxies, starburst galaxies, gamma-ray bursts, and magnetars.

These extragalactic astrophysical objects are distributed along the local large scale structure, most evidently along the “supergalactic plane.” Nearby AGNs are clustered and concentrated around Large Scale Structures (LSS) with a typical clustering length of 5–15 Mpc. The typical amplitude of such AGN concentrations is estimated to be a few hundred percent of the averaged density within a 20° radius circle (Ajello et al. (2012)). This suggests that intermediate-scale anisotropy could have a similar angular scale.

Indeed, the Telescope Array (TA) experiment has observed evidence (at the 3.4σ level) for a Hotspot near Ursa Major for event energies above 57 EeV in Abbasi et al. (2014a). This anisotropy has a maximum significance in a 20 degree circle centered on 9^h48^m , 43° .

The present paper is an extension to lower energies ($E < 57$ EeV) and is specifically a search for differences in the energy distribution of events everywhere within the field of view.

2. EXPERIMENT

The TA experiment in Millard County, Utah (39.3° N, 112.9° W) consists of a surface detector (SD) array (Abu-Zayyad et al. (2013a)) and three fluorescence detectors (FD) (Tokuno et al. (2012)). The SD array has 507 plastic scintillation detectors each 3 m^2 in area placed on an square grid with a spacing of 1.2 km resulting in a 700 km^2 array area. This collection area makes it the largest cosmic-ray detector in the northern hemisphere. Data has been collected since 2008 with a close to 100% duty cycle. Less than 10% of SD data is observed in coincidence with the FD and this hybrid data is used to calibrate the energy scale of the SD using the calorimetric fluorescence technique.

3. DATA SET

For this analysis, SD data recorded between 2008 May 11 and 2015 May 11 is used. Events are reconstructed in the same manner as the “Hotspot” analysis of Abbasi et al. (2014a). The energy of reconstructed events is determined by the SD array and renormalized by 1/1.27 to match the calorimetrically determined energy scale of the FD (Abu-Zayyad et al. (2013b)). The cuts are tighter than the previous Hotspot paper to improve the zenith angle resolution at lower energies (Abbasi et al. (2014a)).

The cuts applied are as follows:

1. Energy $\geq 10^{19.0}$ eV. Detection efficiency is $\sim 100\%$ above this energy.

* Deceased

2. Each event triggered at least four SDs.
3. Event arrival direction zenith angle $< 55^\circ$.
4. Reconstructed event pointing direction error $< 5^\circ$.
5. Event core distance from array boundary > 1.2 km.
6. Shower lateral distribution fit $\chi^2/dof < 10$.

After cuts, there are a total of 3027 events in the data set.

The azimuthal angle distribution is in very good agreement with the theoretical flat distribution and the zenith angle distribution is in good agreement with the theoretical $g(\theta) = \sin(\theta)\cos(\theta)$ distribution. The energy spectrum is also in good agreement with the published spectrum (Abu-Zayyad et al. (2013b); Abbasi et al. (2015)).

The energy resolution and zenith angle resolution of events in the data set range from 10 to 20% and 1.0° to 1.5° respectively, depending on core distance from the array boundary and improve with increasing energy. These resolutions are sufficient to search for intermediate-scale cosmic-ray energy anisotropy.

4. MONTE CARLO DESCRIPTION

Each Monte Carlo (MC), and data event, is defined by four variables - energy, zenith angle, azimuthal angle, and time. The latitude and longitude are defined from the center of the Telescope Array at 39.3° Long., 112.9° Lat. These variables are used to calculate the Right Ascension (R.A.) and Declination (Dec.) in equatorial coordinates for each event (Vallado (2007)).

The energy distribution of each MC set is sampled by interpolation from a large set of MC events reconstructed through an SD simulation which takes into account detector acceptance, on-time, and bias in the energy spectrum. The energy spectrum of this large MC set is the average HiRes spectrum (Abbasi et al. (2008)) and was used for the TA spectrum measurement in Ivanov (2012). The same cuts applied to the data are applied to these simulated events. There are 386,125 MC events with energies $E \geq 10^{19.0}$ eV, 250,742 with $E \geq 10^{19.1}$ eV, with 112,405 $E \geq 10^{19.2}$ eV, and 103,912 with $E \geq 10^{19.3}$ eV.

The spacial variables of the isotropic MC events are thrown with a uniform azimuth distribution and geometrical zenith angle distribution of $g(\theta) = \sin(\theta)\cos(\theta)$. On-time is simulated by randomly sampled trigger times from a large set of 246,499 data events with $E > 10^{17.7}$ eV.

The result is that each set of isotropic MC events simulates the expected data given the detector configuration, and on-time, with no anisotropies. These MC sets are used to calculate the final significance of any data anisotropy.

5. METHOD

5.1. Oversampling Anisotropy

The oversampling method used in this analysis is a modification of the type of analysis that was developed by the AGASA collaboration to search for large-scale anisotropy (Hayashida et al. (1999a); Hayashida et al. (1999b)), namely a statistical analysis done within overlapping spherical cap bins on the sky. The TA and HiRes collaborations have used similar methods previously in Abbasi et al. (2014a), Kawata et al. (2013), and Ivanov & Thomson (2008)).

5.1.1. Grid

Here the oversampling is done on a grid of points with a median equal opening angle spacing of $0.5^\circ \pm 0.04^\circ$ between any other adjacent point. This equal opening angle spacing ensures equal sampling of the area in the oversampled sky and minimizes declination dependent bias. While the field of view extends to -16° , the grid is stopped at 10° to avoid problems with the size of the spherical cap bins described in the next section.

5.1.2. Equal Exposure Spherical Caps

There is a sample size bias in distribution tests of flux, such as χ^2 's and likelihood ratios, which creates a declination bias in the calculated significances if the expectation sample size changes greatly with declination. Due to the geometrical zenith angle exposure $g(\theta) = \sin(\theta)\cos(\theta)$ just such a bias is created if the spherical cap bin sizes are constant. An equal exposure binning is adopted such that, at each point of the oversampling grid, the MC calculated exposure ratio $\alpha = N_{on}/N_{off}$ (Gillessen & Harney (2005)) is a constant value.

A 2×10^7 MC event set is used to determine the three parameter fit of the bin sizes on the grid, the average bin size (15.0° , 20.0° , 25.0° , and 30.0°), and the constant α exposure ratio that results in the required average bin size.

Smaller bin sizes do not have enough statistics inside them and larger bin sizes start to lose sufficient statistics outside for a distribution comparison. It is also the case that a 35° bin size covers more than 50% of the oversampling grid and is no longer “intermediate-scale.” Furthermore, the larger the bin size the more it changes shape at the lowest declinations due to being cut off by the exposure limit.

After the nominal bin sizes are found each exposure ratio α map is calculated using a set of 5×10^7 MC events to account for any remaining small variations in the bin size fit.

Figure 1 shows the constant exposure ratio binning of $\alpha = 14.03\%$. Ratios of 3.35%, 6.04%, 9.58%, and 14.03% were tested to maximize the data pre-trial significance (these ratios have spherical cap bin size averages of 15.0° to 30.0°).

The exposure ratio that maximizes the data pre-trial significance is 14.03% which is an average spherical cap bin size of

30.0°. This is a free parameter that the post-trial significance calculation takes into account.

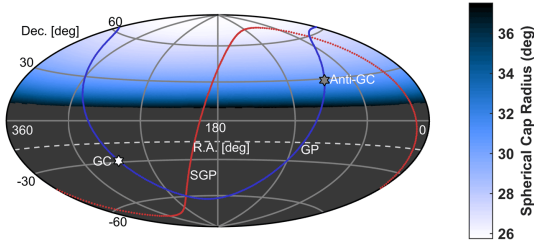


Figure 1. Equatorial Hammer-Aitoff projection of spherical cap bin sizes with a Monte Carlo (MC) defined exposure ratio of $\alpha = N_{on}/N_{off} = 14.03\%$ at each grid point. The average spherical cap bin radius is 30.0°. The dashed curve at Dec. = -16° defines the FoV.

5.2. Energy Distribution Comparison Test

To calculate the significance of a localized deviation in the energy spectrum the binned Poisson likelihood goodness of fit (GOF) test (Baker & Cousins (1984); Olive et al. (2014)) is used to compare the energy distribution inside a spherical cap to the distribution of all events outside the cap. This test was used previously by TA in a composition paper for comparing X_{max} distributions (Abbasi et al. (2014b)). It is a GOF test that allows a low number of events in each energy bin, for both the observed (N_{on} inside the spherical cap bins), and the expected (N_{bg} normalized events outside) energy distributions.

Equation 1a shows this test in terms of observed energy histogram bin frequencies, n_i , expected bin frequencies, μ_i , and the exposure ratio α . The local pre-trial σ significance is calculated by approximating the Poisson likelihood ratio as $-\chi^2/2$ with degrees of freedom $dof = \#bins + 2$. The two additional degrees of freedom come from the estimated background calculation and the combining of low statistic energy bins as described below. This was tested and confirmed to follow the correct χ^2 distribution by MC simulation.

$$\chi^2 \simeq 2 \sum_i \mu_i - n_i + n_i \ln(n_i/\mu_i) \quad (1a)$$

$$N_{on} = \sum_i n_i \quad (1b)$$

$$N_{bg} = \sum_i \mu_i = \alpha(N_{events} - N_{on}) \quad (1c)$$

The *a priori* choice of the energy binning is based on the energy resolution of the detector and is chosen to be slightly smaller than the average resolution for energies

$10^{19} \leq E \leq 10^{20.4}$ eV. This results in an energy bin width of $0.05 \log_{10}(E/\text{eV})$.

If the expected number of events in an energy bin is less than 1 ($\mu_i < 1$) it is combined with alternating adjacent bins. The resulting smallest energy bin expectations are greater than 2 ($\mu_i > 2$). The combining of bins with $\mu_i < 1$ ensures that the bias is positive for all bins instead of negative for the high energy bins with small expectations. The bias against the exact, single bin χ^2 , distribution is less than +15% for $\mu_i > 2$, and drops to +5% at expectations of 5 events in a bin (Heinrich (2001)). This bias is smaller than other possible tests, is present for all locations on the sky map, and also present in the MC trials when calculating the global post-trial significance.

The expected energy spectrum is defined as the histogram of events outside the spherical cap bin (N_{off}) normalized to the expected number of events inside the cap bin (N_{bg}). The expected number of events inside the cap bins is calculated using the method of Li & Ma (1983).

At each point of the oversampling grid the exposure ratio $\alpha = N_{on}/N_{off}$ is calculated from a set of 5×10^7 isotropic MC events. The background calculated from the data is $N_{bg} = \alpha N_{off} = \alpha(N_{events} - N_{on})$ and therefore varies depending on the magnitude of N_{on} inside each spherical cap bin (Gillessen & Harney (2005)).

The lowest energy threshold tested to maximize the data pre-trial significance was $10^{19.0}$ eV as this is the minimum energy for which detection efficiency is $\sim 100\%$. With only 546 events the statistics above $10^{19.4}$ eV are not sufficient for an energy spectrum anisotropy analysis. The maximum significance was found to be for energies $E \geq 10^{19.2}$ eV. This is treated as a free parameter and appropriate penalty factors for this scan are taken, as described in Section 6.3.

Above $10^{19.2}$ eV there are 1332 events in the data set; 1248 with energy $10^{19.2} \leq E < 10^{19.75}$ eV and 84 with $E \geq 10^{19.75}$ eV. The energy threshold of $10^{19.75}$ eV (more exactly 57 EeV) was used for the TA Hotspot analysis and corresponds to the lower energy threshold determined by the AGN correlation results from PAO in Abu-Zayyad et al. (2013c). Due to the tighter cuts there are less events in this energy range than in the Hotspot analysis.

6. RESULTS

6.1. Density Map

Figure 2(a) shows an equatorial coordinate sky map of the 1332 cosmic-ray events in the data set observed by the TA SD array with energy $E \geq 10^{19.2}$ eV. The oversampled number of events, N_{on} , using the equal opening angle sampling grid, and spherical cap bin size average of 30° (Figure 1), discussed in Section 5.1 is shown in Figure 2(b).

6.2. Local Energy Anisotropy Significance

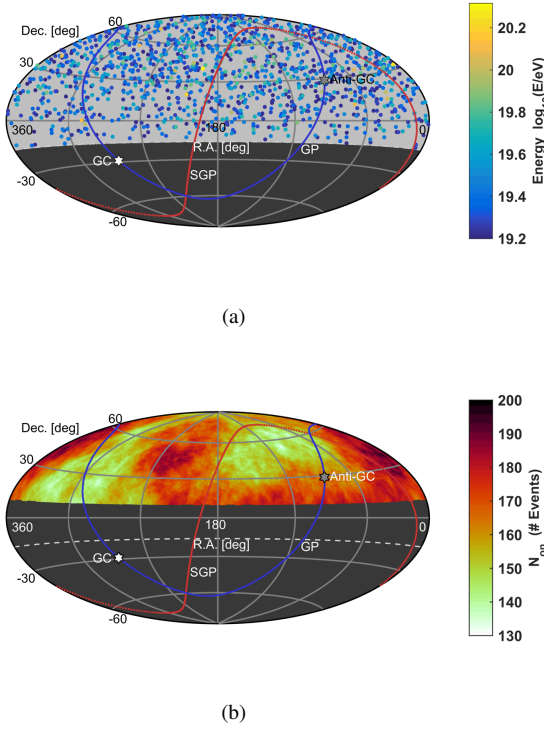


Figure 2. Equatorial Hammer-Aitoff projections of UHECR events in the data set. (a) Scatter plot of events where the colors are $\log_{10}(E/\text{eV})$. There is a visible deficit of events at the location of the previously reported Hotspot ($9^{\text{h}}48^{\text{m}}, 43^{\circ}$). (b) Number of observed events, N_{on} , at each grid point, inside 14.03% equal exposure bins of the radius shown in Figure 1. The dashed curve at $\text{Dec.} = -16^{\circ}$ defines the FoV. Solid curves indicate the galactic plane (GP) and supergalactic plane (SGP). White and grey hexagrams indicate the Galactic center (GC) and anti-galactic center (Anti-GC) respectively.

Using the method outlined in Section 5.2 the pre-trial significance of local relative energy distribution deviations is calculated. Inside each spherical cap bin the energy distribution of events (N_{on}) is compared to that outside (N_{off}). In the binned Poisson likelihood goodness of fit test (Equation 1a), the μ_i histogram bin frequencies are the N_{off} energy histogram frequencies normalized to the expected number of events (N_{bg}) calculated using Equation 1c. The α parameter is the Monte Carlo (MC) calculated exposure ratio described in Section 5.1.2.

The resulting local pre-trial energy distribution anisotropy significance is shown in Figure 3 using the spherical cap bin average of 30° and $E \geq 10^{19.2}$ eV. The maximum pre-trial significance is $6.17\sigma_{\text{local}}$ at $9^{\text{h}}16^{\text{m}}, 45^{\circ}$ inside a spherical cap bin of radius 28.43° . This is 7° away from the previously published Hotspot location in Abbasi et al. (2014a).

The histogram of events inside the spherical cap bin at maximum significance compared to the histogram of ex-

pected energies is shown in Figure 4 with, and without, the rebinning discussed in Section 5.2. Individual bin contributions to the statistical significance from a Hotspot excess of events $E > 10^{19.75}$ eV (27 observed and 8 expected, $\chi^2/\text{dof} = 38.1/4.5$), and a “Coldspot” deficit $10^{19.2} \leq E < 10^{19.75}$ eV (120 observed and 158 expected, $\chi^2/\text{dof} = 40.2/11.5$). The deficit is larger in magnitude than the excess as the expected number of events is $N_{\text{bg}} = 166.2$ and the observed number of events $N_{\text{on}} = 147$.

6.3. Global Significance

To calculate the global post-trial significance a scan penalty must be taken for the four minimum energy cuts ($10^{19.0}$, $10^{19.1}$, $10^{19.2}$, and $10^{19.3}$ eV) and 4 equal exposure ratio spherical cap bin sizes (3.35%, 6.04%, 9.58%, and 14.03%) that were tested to maximize the data binned Poisson likelihood GOF σ_{local} shown in Figure 3.

The isotropic MC simulations, as described in Section 4, are created with the same number of events as the data for each low energy threshold. The scanned variables are applied to each MC set to create 16 binned Poisson likelihood σ_{local} maps. The maximum σ_{local} significance at any grid point on all 16 maps is considered as one MC for counting MC sets that have a higher significance than the data.

2.5×10^6 sets of these 16 maps were created to calculate the post-trial global significance. The empirical probability density function (PDF) of these MC sets maximum σ ’s is shown in Figure 5.

There were 232 MC out of 2.5×10^6 with a higher maximum significance than 6.17σ . This corresponds to a global post-trial one-sided significance of $3.74\sigma_{\text{global}}$

6.4. Systematic Checks

There is a systematic bias on the UHECR energy determination due to seasonal and daily temperature induced changes in the average lateral distribution of particles in cosmic ray extensive air showers. This bias is estimated to fluctuate, about $\pm 7\%$, with a negative bias in the winter months and positive in the summer. There is also an estimated fluctuation of about $\pm 5\%$ throughout each 24 hour period. Applying these estimated energy corrections to the data results in a lowering of the local significance by about 0.05σ .

In calculating the equal exposure binning, the α exposure ratio, and the global significance, the trigger times of events with energies $E \geq 10^{17.7}$ eV were sampled to create the MC sets. This is to accurately model how the TA SD array would see an isotropic sky. It is known however that the acceptance, and therefore the trigger time distribution, is dependent on energy. To test the effect of this sampling method MC sets were also created using completely uniform event trigger times and the entire calculation redone. The result is an increase in the pre-trial, and post-trial, significance of 0.04σ .

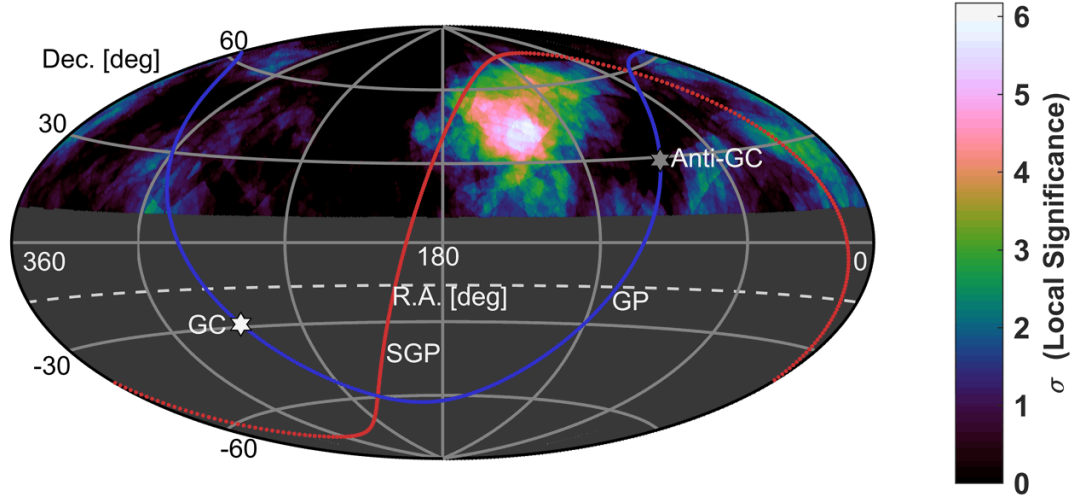


Figure 3. Projection of the local pre-trial energy spectrum anisotropy significance, for each 14.03% equal exposure spherical cap bin ($E \geq 10^{19.2}$ eV). The maximum significance is $6.17\sigma_{local}$ at $9^h 16^m, 45^\circ$. This is 7° from the previously published Hotspot location in Abbasi et al. (2014a). The dashed curve at Dec. = -16° defines the FoV. Solid curves indicate the galactic plane (GP) and supergalactic plane (SGP). White and grey hexagrams indicate the Galactic center (GC) and anti-galactic center (Anti-GC).

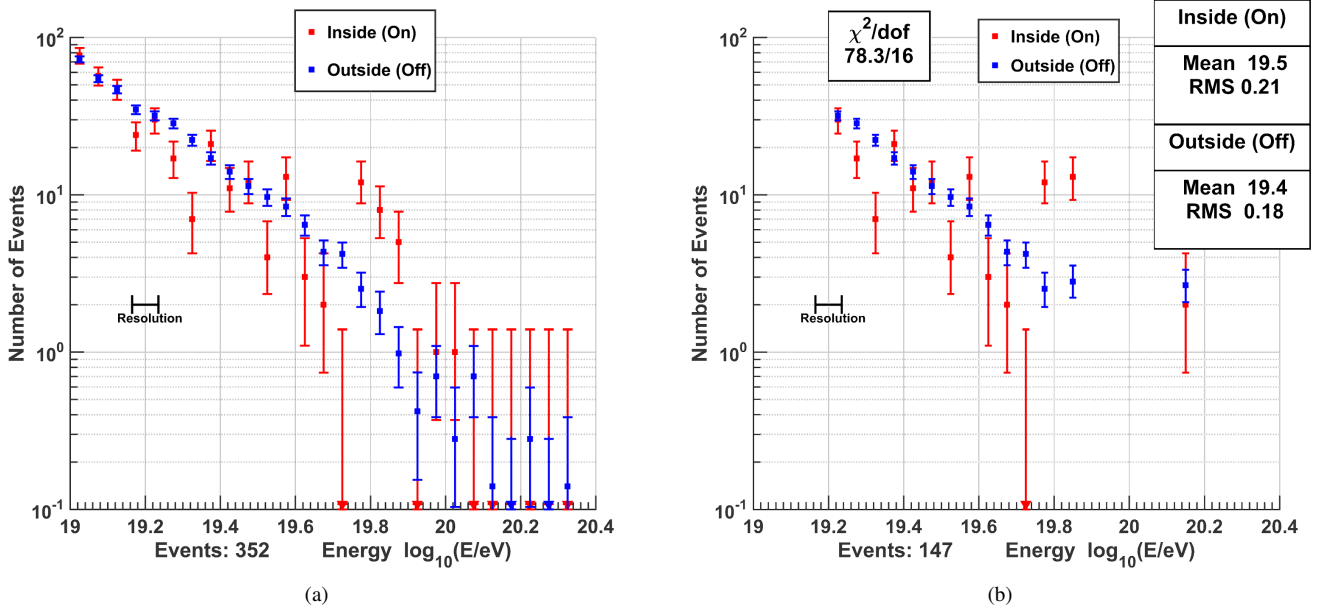


Figure 4. Energy histograms, at the point of maximum significance ($9^h 16^m, 45^\circ$), of events inside the spherical cap bin of radius 28.43° (red) compared to the expected energies (blue). (a) Before automatic rebinning for events with energies $E > 10^{19.0}$ eV. (b) After rebinning for events with energies $E > 10^{19.2}$ eV (the energy threshold that maximizes the significance). There are 147 events while the expected number is $N_{bg} = 166.2$. There are only three out of 11 bins for $E < 10^{19.75}$ eV above expectation.

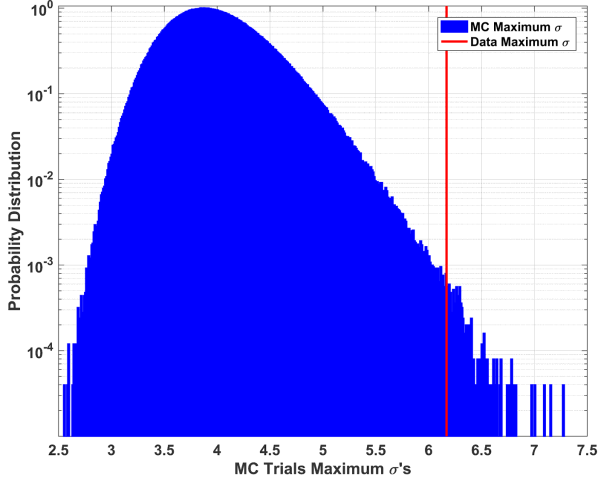


Figure 5. The empirical probability density function of the maximum local σ 's for all 2.5×10^6 MC trials. The area under the distribution above $6.17\sigma_{local}$ corresponds to a $3.74\sigma_{global}$ post-trial significance for the measured energy spectrum anisotropy.

In addition to the seasonal energy correction test the energy distribution of events was also considered in anti-sidereal coordinates. This is an artificial coordinate system which emphasizes seasonal effects. No evidence for an energy spectrum anisotropy is found in anti-sidereal coordinates as would be expected for an anisotropy.

Other systematic checks include comparing the shower geometry variable (azimuth, zenith, core position etc.) distributions inside the anisotropic area, to outside, and show no disagreements (nor are there disagreements between the different energy ranges inside the area) – they all also agree with isotropic MC simulation. The R.A., trigger time, and Dec. distributions inside the spherical cap are in very good agreement between the Hotspot energy range events and the Coldspot energy range events – they also each agree with isotropic MC. Also, the full energy distributions inside, and outside, the spherical cap do not show any significant seasonal variation.

7. DISCUSSION

The location of the maximum energy anisotropy is centered near the supergalactic plane which contains local galaxy clusters such as the Ursa Major cluster (20 Mpc from Earth), the Coma cluster (90 Mpc), and the Virgo cluster (20 Mpc). The closest angular distance between the hot/cold center and the supergalactic plane is 22° which is 3 degrees larger than the previously determined Hotspot alone and is in the vicinity of the Ursa Major cluster. The difference is not statistically significant given the oversampling bin sizes and Gaussian fit to the Hotspot events as shown in Abbasi et al. (2014a).

To get an idea if the measured energy spectrum anisotropy is correlated with the supergalactic plane the locations, with this hot/cold (excess/deficit) behavior, in Figure 3 are converted to supergalactic coordinates and fit to a straight line (weighted by the pre-trial σ^2). The result corresponds to a great-circle rotated in declination by $-16.5 \pm 0.1^\circ$ and tilted $2 \pm 1^\circ$ around the center of the fit. This is suggestive of an extended feature that could be correlated with supergalactic structure. Possible mechanisms for producing such a shift include focusing of cosmic ray flux by supergalactic magnetic sheets, which have an effect for events with $E > 50$ EeV, that have been discussed in Biermann et al. (1997), and deflection of lower energy background events transverse to the sheet as discussed in Ryu et al. (1998).

This feature may also be associated with the closest galaxy groups and/or the galaxy filament connecting us with the Virgo cluster (Dolag et al. (2004); He et al. (2016); Pfeffer et al. (2017)), if UHECR are protons as indicated by previous TA studies such as Abbasi et al. (2014b). If the anisotropic cosmic rays are heavy nuclei, they may originate near the supergalactic plane and be deflected by extragalactic magnetic fields (EGMF) and the galactic magnetic halo field (GMF) (Tinyakov & Tkachev (2002); Takami et al. (2012)). If magnetic deflection or focusing is the mechanism, the magnitude is expected to be energy dependent.

To determine the origin of this feature, we will need greater UHECR statistics in the northern sky. Better information about the mass composition of the UHECRs, GMF, and EGMF would also be important. The TA detector is currently being expanded by a factor of four (TAx4 Sagawa (2013)) and five years of additional data with this expanded detector should allow us to answer these questions.

8. SUMMARY

Using seven years of TA SD ultra-high energy cosmic ray (UHECR) events a feature has been found appearing as a deficit of lower energy events ($10^{19.2} \leq E < 10^{19.75}$ eV) and an excess of high energy events ($E \geq 10^{19.75}$ eV) in the same region of the sky. The maximum local pre-trial significance is 6.17σ and appears at $9^h 16^m, 45^\circ$. The global post-trial probability of an energy spectrum anisotropy of this significance appearing by chance in an isotropic cosmic ray sky was found to be 9×10^{-5} ($3.74\sigma_{global}$). This feature is suggestive of energy dependent magnetic deflection of UHECR events.

The Telescope Array experiment is supported by the Japan Society for the Promotion of Science through Grants-in-Aid for Scientific Research on Specially Promoted Research (21000002) “Extreme Phenomena in the Universe Explored by Highest Energy Cosmic Rays” and for Scientific Research (19104006), and the Inter-University Research Program of the Institute for Cosmic Ray Research; by the U.S.

National Science Foundation awards PHY-0601915, PHY-1404495, PHY-1404502, and PHY-1607727; by the National Research Foundation of Korea (2015R1A2A1A01006870, 2015R1A2A1A15055344, 2016R1A5A1013277, 2007-0093860, 2016R1A2B4014967); by the Russian Academy of Sciences, RFBR grant 16-02-00962a (INR), IISN project No. 4.4502.13, and Belgian Science Policy under IUAP VII/37 (ULB). The foundations of Dr. Ezekiel R. and Edna Wattis Dumke, Willard L. Eccles, and George S. and Dolores Doré Eccles all helped with generous donations. The State of Utah supported the project through its Economic Development Board, and the University of Utah through the Office of the Vice President for Research. The experimental site became available through the cooperation of the Utah School and Institutional Trust Lands Administration

(SITLA), U.S. Bureau of Land Management (BLM), and the U.S. Air Force. We appreciate the assistance of the State of Utah and Fillmore offices of the BLM in crafting the Plan of Development for the site. Patrick Shea assisted the collaboration with valuable advice on a variety of topics. The people and the officials of Millard County, Utah have been a source of steadfast and warm support for our work which we greatly appreciate. We are indebted to the Millard County Road Department for their efforts to maintain and clear the roads which get us to our sites. We gratefully acknowledge the contribution from the technical staffs of our home institutions. An allocation of computer time from the Center for High Performance Computing at the University of Utah is gratefully acknowledged.

REFERENCES

- Abbasi, R. U., et al. 2008, *PhRvL*, 100, 101101.
<https://arxiv.org/abs/astro-ph/0703099>
- . 2014a, *ApJ*, 790, L21. <https://arxiv.org/abs/1404.5890>
- . 2014b, *Astropart. Phys.*, 64, 49.
<https://arxiv.org/abs/1408.1726>
- . 2015, *Astropart. Phys.*, 68, 27. <https://arxiv.org/abs/1410.3151>
- Abu-Zayyad, T., et al. 2013a, *Nucl. Instrum. Meth.*, A689, 87.
<https://arxiv.org/abs/1201.4964>
- . 2013b, *ApJ*, 768, L1. <https://arxiv.org/abs/1205.5067>
- . 2013c, *ApJ*, 777, 88. <https://arxiv.org/abs/1306.5808>
- Ajello, M., Alexander, D. M., Greiner, J., et al. 2012, *ApJ*, 749, 21.
<https://arxiv.org/abs/1202.3137>
- Baker, S., & Cousins, R. D. 1984, *Nucl. Instr. Meth. Phys. Res.*, 221, 437
- Biermann, P. L., Kang, H., & Ryu, D. 1997, 9 p.
<https://arxiv.org/abs/astro-ph/9709250>
- Dolag, K., Grasso, D., Springel, V., & Tkachev, I. 2004, *J. Korean Astron. Soc.*, 37, 427
- Gillessen, S., & Harney, H. L. 2005, *A&A*, 430, 355.
<https://arxiv.org/abs/astro-ph/0411660>
- Hayashida, N., et al. 1999a, *Astropart. Phys.*, 10, 303.
<https://arxiv.org/abs/astro-ph/9807045>
- Hayashida, N., et al. 1999b, in *Proceedings, 26th ICRC, Salt Lake City, August 17-25*.
http://krusty.physics.utah.edu/~icrc1999/root/vol3/o1_3_04.pdf
- He, H.-N., Kusenko, A., Nagataki, S., et al. 2016, *PhRvD*, D93, 043011. <https://arxiv.org/abs/1411.5273>
- Heinrich, J. G. 2001, *CDF, Note 5718*
- Ivanov, D. 2012, PhD thesis, Rutgers, the State University of New Jersey. http://www.telescopearray.com/images/papers/theses/thesis_ivanov_rev2016.pdf
- Ivanov, D., & Thomson, G. B. 2008, *ICRC*, 4, 445
- Kawata, K., Fukushima, M., & D., I. 2013, in *Proceedings, 33rd ICRC (ICRC2013): Rio de Janeiro, Brazil, July 2-9, 0311*.
<http://www.cbpf.br/~icrc2013/papers/icrc2013-0311.pdf>
- Kotera, K., & Olinto, A. V. 2011, *ARA&A*, 49, 119.
<https://arxiv.org/abs/1101.4256>
- Li, T. P., & Ma, Y. Q. 1983, *ApJ*, 272, 317
- Olive, K. A., et al. 2014, *Chin. Phys.*, C38, 090001
- Pfeffer, D. N., Kovetz, E. D., & Kamionkowski, M. 2017, *Mon. Not. Roy. Astron. Soc.*, 466, 2922.
<https://arxiv.org/abs/1512.04959>
- Ryu, D., Kang, H., & Biermann, P. L. 1998, *A&A*, 335, 19.
<https://arxiv.org/abs/astro-ph/9803275>
- Sagawa, H. 2013, in *Proceedings, 33rd ICRC (ICRC2013): Rio de Janeiro, Brazil, July 2-9, 0121*.
<http://www.cbpf.br/~icrc2013/papers/icrc2013-0121.pdf>
- Takami, H., Inoue, S., & Yamamoto, T. 2012, *Astropart. Phys.*, 35, 767. <https://arxiv.org/abs/1202.2874>
- Tinyakov, P. G., & Tkachev, I. I. 2002, *Astropart. Phys.*, 18, 165.
<https://arxiv.org/abs/astro-ph/0111305>
- Tokuno, H., et al. 2012, *Nucl. Instrum. Meth.*, A676, 54.
<https://arxiv.org/abs/1201.0002>
- Vallado, D. A. 2007, *Fundamentals of Astrodynamics and Applications* (Springer-Verlag New York), 1055.
<https://books.google.com/books?id=PJLIWzMBKjkC>